Journal of Crystal Growth 592 (2022) 126734

Contents lists available at ScienceDirect

Journal of Crystal Growth

journal homepage: www.elsevier.com/locate/jcrysgro

Effect of hyaluronic acid on the struvite crystallization: A structural, morphological, and thermal analysis study

Sevgi Polat [a,b,*], Huseyin Burak Eral [a]

[a] Process & Energy Department, Faculty of Mechanical, Maritime and Materials Engineering, Delft University of Technology, 2628 CB Delft, The Netherlands
[b] Chemical Engineering Department, Faculty of Engineering, Marmara University, 34854 İstanbul, Turkey

ARTICLE INFO

Communicated by Alexander van Driessche

Keywords:
B1. Struvite
B1. crystallization
A1. shape parameters
A1. TGA/FTIR
A1. thermal kinetics

ABSTRACT

The struvite crystals constitute one of the common types of urinary stones. Such stones are also referred as "infection stones" due to their tendency to cause infections in urinary tract. A considerable effort has been placed to identify natural or synthetic crystal-growth modifiers for this kind of urinary stone in literature, yet macromolecules commonly found in urine have been underexplored. In the present study, we experimentally focus on how hyaluronic acid, a protein commonly found in urine, alters the struvite crystallization in aqueous solution and in an artificial urine media. By gradually adding ammonium dihydrogen phosphate to a solution containing magnesium chloride hexahydrate, reactive crystallization is carried out in a well-mixed and thermostated vessel at 37 °C. The resulting struvite crystals are characterized structurally by XRD and FTIR as well as morphologically and in terms of their surface charge. In addition, the thermal decomposition behavior of the struvite with and without hyaluronic acid and released volatile products were simultaneously investigated using a TGA/FTIR system. The average activation energy calculated using the Friedman method was 49.2 ± 5.1 kJ/mol. The results of the kinetic and thermodynamic analyses showed that decomposition of the struvite crystals was endothermic and followed the multiple stage reaction mechanism.

1. Introduction

Urinary stones are a serious clinical issue that affect nearly 20% of all humans, and the level of recurrence remains at 50% after treatment, with the occurrence increasing among those living in industrialized countries [1]. Urinary stones are formed pathologically through a combination of physical and chemical processes. They are composed of an organic matrix that comprises mainly the crystalline phases of various substances, with different types of stones appearing based on different factors and materials [2,3]. Magnesium ammonium phosphate hexahydrate ($MgNH_4PO_4{\cdot}6H_2O$), also known as "struvite", is made up of magnesium, ammonium and phosphate in an equimolar (1:1:1) ratio. 10–30% of all urinary stones have struvite as the main inorganic component. These struvite stones are also called "Infection stones" which is a result of the activity of microorganisms producing urease [4]. These microorganism causes an infection mainly from *Proteus* species [5,6]. Urease, a bacterial enzyme, catalyzes the hydrolysis of urea to form ammonia, which then increases urine pH and elevates concentrations of ammonium (NH_4^+), carbonate (CO_3^{2-}), and phosphate (PO_4^{3-}) ions, which combine with magnesium (Mg^{2+}) ions in urine and lead struvite crystallization [7]. Struvite stones, one of the most dangerous, can cause potential life-threatening complications from infection [8–10]. Extracorporeal shock wave lithotripsy is frequently used to treat urinary stones; however, it is not a permanent solution as the recurrence after treatment remains at 50% [11]. In addition, several drugs have been reported to effectively mitigate other stone types; however, these treatments for infection stones have not yet been resolved. Although several studies on the formation of struvite urinary stones are reported in the literature [5,12,13], more research is necessary to develop a non-invasive treatment alternative to extracorporeal shock wave lithotripsy. In-vivo studies point out that organic and inorganic modifiers, which are additives that promote or inhibit crystallization, interact with struvite crystals by adsorbing onto the crystal's surface [14–18]. Studying the influence of these modifiers, especially those that are biocompatible, on the precipitation of struvite may inform development of the treatments for mitigate disease stones. Studies [19–21] have pointed out that the presence of hyaluronic acid in urine plays an important role in the formation of renal stone. Despite the reports pointing out that hyaluronic

* Corresponding author at: Process & Energy Department, Faculty of Mechanical, Maritime and Materials Engineering, Delft University of Technology, 2628 CB Delft, The Netherlands.
E-mail addresses: S.Polat@tudelft.nl (S. Polat), H.B.Eral@tudelft.nl (H.B. Eral).

https://doi.org/10.1016/j.jcrysgro.2022.126734
Received 2 March 2022; Received in revised form 16 May 2022; Accepted 19 May 2022
Available online 23 May 2022

acid alters the crystallization of calcium oxalate [22–24], the most common kidney stone type, its influence on the structural and morphological properties of struvite crystals has not been fully investigated. In particular, there has been no comprehensive kinetic and thermodynamic analysis of struvite using coupled TGA/FTIR system. Taking all this into consideration, the present study focused on the effect of hyaluronic acid as a crystal modifier for struvite and a potent inhibitor of struvite crystallization in vitro. To that end, we characterized emerging crystals structurally and morphologically in aqueous solution and artificial urine detail. Moreover, the thermal decomposition kinetic and thermodynamic parameters of the struvite crystals were determined by a combined method of master plots and the Friedman method. Thereafter, the activation energy and thermodynamic parameters for the crystals were estimated. The present study will provide important information that focuses on the thermal characteristics, kinetics, and thermodynamics of struvite crystals based on TGA/FTIR system to contribute to a better understanding of these characteristics.

2. Materials and methods

2.1. Materials

Magnesium chloride hexahydrate ($MgCl_2{\cdot}6H_2O$), ammonium dihydrogen phosphate ($NH_4H_2PO_4$) used as reactants were analytically pure and obtained from Merck (Darmstadt, Germany). Hyaluronic acid (CAS number 9067–32-7) used as a modifier was obtained from Sigma Aldrich (Gillingham, UK). Deionized water was used to prepare the solutions.

2.2. Experimental method

The struvite crystallization experiment was conducted using a 500-mL glass crystallizer equipped with a thermal jacket for temperature control and a mechanical stirrer equipped with a three-bladed propeller. The temperature of the suspension was kept constant using a thermostat with an accuracy of 0.1 °C. To monitor and keep the pH constant, a pH meter was coupled with an automated pH control device, and the solution was adjusted to pH 8.0 ± 0.1 using sodium hydroxide solution. The experiments were conducted at 37 °C and 300 rpm in both aqueous solution and artificial urine media. The artificial urine was prepared using the method described in literature [25,26] and its content was as follows: 0.01695 M Na_2SO_4, 0.00385 M $MgSO_4{\cdot}7H_2O$, 0.0455 M NH_4Cl, 0.0637 M KCl, 0.1055 M NaCl, 0.0323 M NaH_2PO_4, and 0.00321 M $Na_3C_6H_5O_7$.

To synthesize the struvite crystals, 250 mL 0.1 M magnesium chloride hexahydrate solution was placed into the crystallizer at the beginning of the experiments and left to reach thermal equilibrium. Then, a peristaltic pump was used to feed 250 mL 0.1 M ammonium dihydrogen phosphate solution into the crystallizer at a rate of 5 mL/min. At all times, the crystallizer cover was kept closed. After the reactant-feeding operation was complete, the sample suspension was removed, quickly filtered using a vacuum filter, washed with distilled water, and dried in an oven at 30 °C. These prepared samples were then used for further analysis.

Hyaluronic acid was used as a modifier to investigate its effects on the struvite crystals at specific concentrations. Specific amounts of the modifier were added to the $MgCl_2{\cdot}6H_2O$ solution before adding the ammonium dihydrogen phosphate ($NH_4H_2PO_4$) solution. The hyaluronic acid was applied at concentrations of 0, 0.025, and 0.25 mM.

2.3. Analysis

X-ray diffraction (XRD) analysis was performed to determine the crystal structure using a Bruker D2 Phaser table-top diffractometer. The phase of measured samples was analyzed using a monochromatic Cu Kα radiation source and a wavelength of 1.5418 Å. The XRD patterns were recorded within the 2θ range of 10 to 70° with 3°/min scanning speed and 30 kV tube voltage. The calculation of unit cell parameters of the crystals was performed on the Materials Analysis Using Diffraction (MAUD) software (developed by Wenk, Matthies & Lutterotti and Ferrari & Lutterotti). The functional groups of struvite were characterized by Fourier transform infrared (FTIR) spectrometer. FTIR spectra were scanned between 4000 and 650 cm^{-1} in transmission mode using a Shimadzu IR Affinity-1 Fourier Transform Infrared Spectrometer. The morphological changes of the struvite were investigated by Zeiss EVO LS 10 scanning electron microscopy working at 15 kV. In addition, the crystals were analyzed using a Malvern Morphologi G3 instrument to gain a better understanding of the size and shape properties of the struvite. All analysis was done with the 10 × lens. The volume-based particle size distribution was measured using the Mastersizer 2000 laser particle size analyzer (Malvern Panalytical, Malvern, UK). The zeta potential (ζ potential) measurements of the struvite crystals were performed using a Malvern Zetasizer Nano ZS instrument. Each test was repeated at least three times with good reproducibility, and the average results used in the current study. The thermal decomposition of the struvite obtained with and without hyaluronic acid was studied using a Setaram LABSYS Evo thermogravimetric analyzer in a nitrogen atmosphere between 25 °C and 325 °C. 10 ± 0.1 mg of sample is used for analysis with a purge gas flow rate of 20 mL/min. Moreover, the kinetic and thermodynamic calculations for struvite crystals were performed using different heating rates of 5, 10 and 20 °C/min. The volatile components released during thermal decomposition were simultaneously identified using TGA/FTIR system. An FTIR spectrometer (Bruker Tensor27) was used in combined with a TGA device that heated at a rate of 20 °C/min.

2.4. Kinetic analysis

Thermogravimetric analysis is used to investigate the behavior of thermal decomposition of solids and to estimate the kinetic parameters, such as the activation energy, and pre-exponential factor for the hydration of the crystal water for the studied struvite crystals.

The basic kinetic equation for solid-state thermal decomposition can be defined as:

$$\frac{d\alpha}{dt} = k(T)f(\alpha) \tag{1}$$

where $f(\alpha)$, $k(T)$, and t represent the reaction model, the reaction rate constant, and time, respectively. The rate constant, $k(T)$, and the conversion, α, are defined in Eq. (2), and Eq. (3), respectively.

$$k(T) = A\exp\left(-\frac{E_\alpha}{RT}\right) \tag{2}$$

where E is the activation energy (kJ/mol), A is the pre-exponential or frequency factor (min^{-1}), T is the absolute temperature (K), and R is the ideal gas constant (8.314 J/mol K).

$$\alpha = \frac{W_0 - W_t}{W_0 - W_f} \tag{3}$$

The terms W_0 and W_f are the initial and final weights, respectively, and W_t is the sample weight at time t. For a constant heating rate, β (K/min) is given by the following equation:

$$\beta = \frac{dT}{dt} \tag{4}$$

For non-isothermal analysis, by substituting Eq. (4) into Eq. (1), the reaction rate can be expressed as:

$$\frac{d\alpha}{dT} = k(T)f(\alpha) = \frac{A}{\beta}\exp(-\frac{E_\alpha}{RT})f(\alpha) \tag{5}$$

Eq. (6) can be obtained by integration:

Table 1
Solid-state kinetic models with corresponding symbols, differential conversion functions *f(α)* and integral conversion functions *g(α)*.

Mechanisms	Symbol	f(α)	g(α)
Order of reaction			
First-order	F_1	$(1-\alpha)$	$-\ln(1-\alpha)$
Second-order	F_2	$(1-\alpha)^2$	$(1-\alpha)^{-1}-1$
Third-order	F_3	$(1-\alpha)^3$	$[(1-\alpha)^{-2}-1]/2$
One and half order	F_4	$(1-\alpha)^{3/2}$	$2[(1-\alpha)^{-1/2}-1]$
Diffusion			
One-way transport	D_1	0.5α	α^2
Two-way transport	D_2	$[-\ln(1-\alpha)]^{-1}$	$\alpha+(1-\alpha)\ln(1-\alpha)$
Three-way transport	D_3	$1.5(1-\alpha)^{2/3}[1-(1-\alpha)^{1/3}]^{-1}$	$[1-(1-\alpha)^{1/3}]^2$
Ginstling-Brounshtein equation	D_4	$1.5[(1-\alpha)^{1/3}-1]^{-1}$	$(1-2\alpha/3)-(1-\alpha)^{2/3}$
Phase boundary reaction models			
Contracting cylinder	R_2	$2(1-\alpha)^{1/2}$	$1-(1-\alpha)^{1/2}$
Contracting sphere	R_3	$3(1-\alpha)^{2/3}$	$1-(1-\alpha)^{1/3}$
Exponential nucleation			
Exponential Law	P_1	$\ln\alpha$	α
Power law, n = 1/2	P_2	$2\alpha^{1/2}$	$\alpha^{1/2}$
Power law, n = 1/3	P_3	$3\alpha^{2/3}$	$\alpha^{1/3}$
Random nucleation and nuclei growth			
Avrami-Erofeev	A_2	$2(1-\alpha)[-\ln(1-\alpha)]^{1/2}$	$[-\ln(1-\alpha)]^{1/2}$
Avrami-Erofeev	A_3	$3(1-\alpha)[-\ln(1-\alpha)]^{2/3}$	$[-\ln(1-\alpha)]^{1/3}$
Avrami-Erofeev	A_4	$4(1-\alpha)[-\ln(1-\alpha)]^{3/4}$	$[-\ln(1-\alpha)]^{1/4}$

$$g(\alpha)=\int_0^{\alpha}\frac{d\alpha}{f(\alpha)}=\frac{A}{\beta}\int_{T_0}^{T}\exp\left(-\frac{E_\alpha}{RT}\right)dT \tag{6}$$

where *g(α)* is the integrated form of the reaction model. The kinetic model *f(α)* is related with a physical model which describes the kinetics. Table 1 illustrates the functional forms of *f(α)* and *g(α)*. The solid reaction mechanism, reflected by the dynamic TGA curves, can be predicted using these expressions.

The *iso*-conversional method, which states that the reaction rates for the solid-state rely only on the temperatures at a constant quantity of conversion, proposed by Friedman method [27] was used in the present study to determine the activation energy of the struvite crystals. This method is a good reliable method because it avoids any mathematical approximations. Its linear equation is represented in Eq. (7).

$$ln\left(\frac{d\alpha}{dt}\right)=ln\left(\beta\left(\frac{d\alpha}{dT}\right)\right)=ln[Af(\alpha)]-\frac{E}{RT} \tag{7}$$

For any given value, the activation energy at any given specific conversion can be determined based on the gradients of the lines obtained from the plot of ln [β(dα/dT)] versus 1/T for Friedman method.

Kissinger's equation [28] given in Eq. (8) was used in this study to estimate the frequency factor (A) for each value of α.

$$A=\frac{\beta E_\alpha\exp(E_\alpha/RT_{peak})}{RT_{peak}^2} \tag{8}$$

The master-plots method, also known as the Criado method [29], was used in combination with the Friedman method to determine kinetic mechanism of solid-state reaction. The master plots method is mathematically represented in Eq. (9).

$$\frac{Z(\alpha)}{Z(0.5)}=\frac{f(\alpha)\times g(\alpha)}{f(0.5)\times g(0.5)}=\left(\frac{T_\alpha}{T_{0.5}}\right)^2\times\frac{(d\alpha/dt)_\alpha}{(d\alpha/dt)_{0.5}} \tag{9}$$

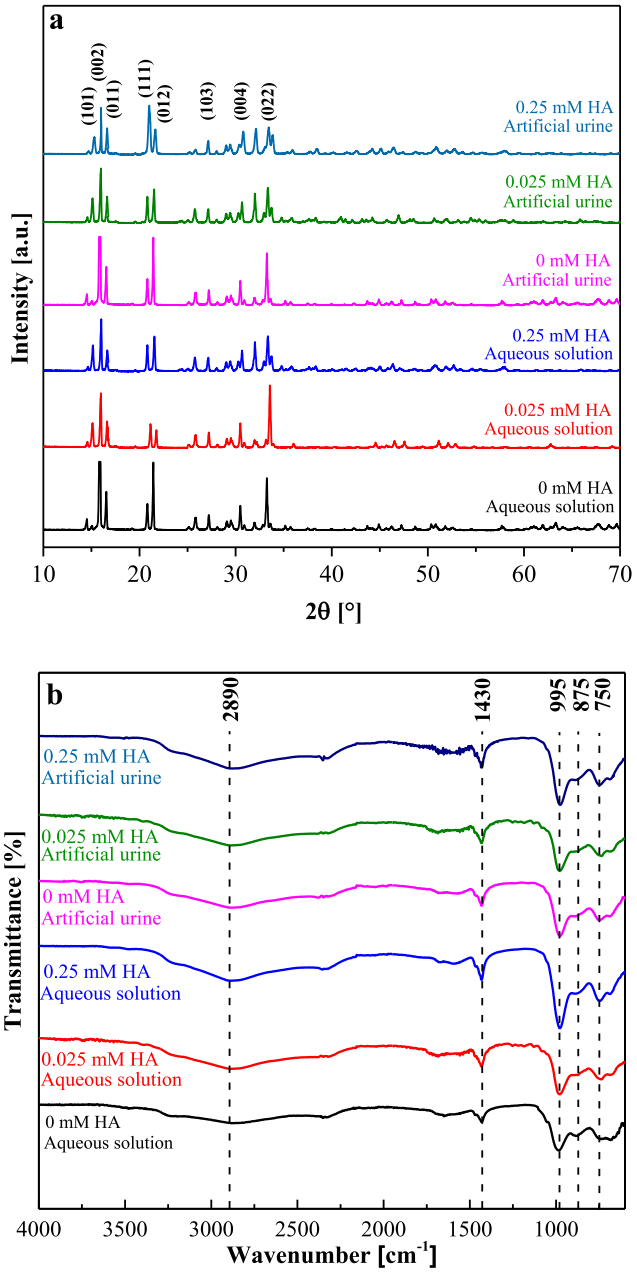

Fig. 1. a) X-ray diffraction (XRD) results and b) Fourier transform infrared (FTIR) results for the struvite crystals obtained in aqueous solution and artificial urine using different concentrations of hyaluronic acid (HA).

Table 2
Unit-cell parameters for the struvite crystals obtained in aqueous solution and artificial urine using different concentrations of hyaluronic acid (HA).

Sample	Unit cell dimensions			
	a (Å)	*b* (Å)	*c* (Å)	*V* (Å)
Aqueous solution without HA	6.944	6.120	11.245	477.88
Aqueous solution with 0.025 mM HA	6.980	6.156	11.249	483.36
Aqueous solution with 0.25 mM HA	6.997	6.173	11.255	486.13
Artificial urine without HA	6.989	6.195	11.271	488.00
Artificial urine with 0.025 mM HA	6.977	6.176	11.262	485.28
Artificial urine with 0.25 mM HA	6.966	6.161	11.242	482.48

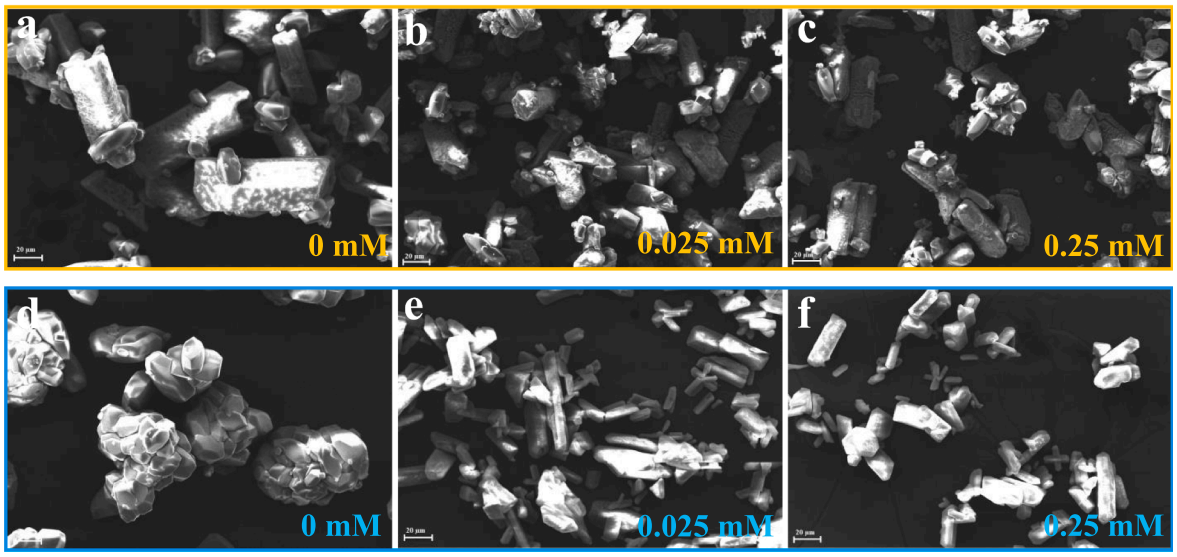

Fig. 2. Scanning electron microscopy (SEM) images for struvite crystals obtained in a) aqueous solution with 0 mM, b) 0.025 mM, and c) 0.25 mM hyaluronic acid and in d) artificial urine media with 0 mM, e) 0.025 mM, and f) 0.25 mM hyaluronic acid.

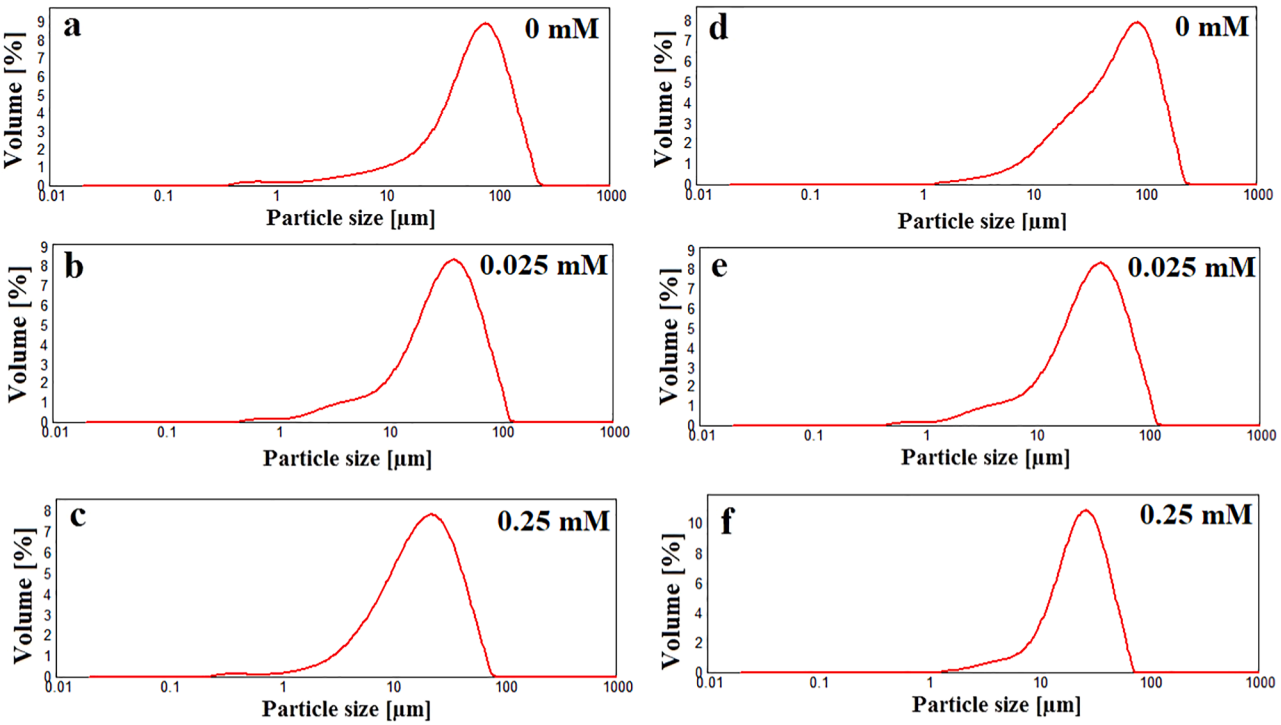

Fig. 3. Particle size distributions of the struvite crystals obtained in a) aqueous solution with 0 mM, b) 0.025 mM, and c) 0.25 mM hyaluronic acid and in d) artificial urine media with 0 mM, e) 0.025 mM, and f) 0.25 mM hyaluronic acid.

We can estimate the predominant reaction mechanism for the thermal decomposition of a solid by comparing theoretical reaction plots with those using experimental data (Table 1).

2.5. Thermodynamic analysis

Eyring equations [30,31] were used to calculate the thermodynamic parameters of the struvite crystals, including enthalpy change (ΔH), Gibbs free energy change (ΔG), and entropy change (ΔS).

$$\Delta H = E_\alpha - RT \tag{10}$$

$$\Delta G = E_\alpha + RT_{peak} \ln\left(\frac{K_B T_{peak}}{hA}\right) \tag{11}$$

$$\Delta S = \frac{\Delta H - T\Delta G}{T_{peak}} \tag{12}$$

Where T_{peak} is the peak temperature of DTG curve, K_B is the Boltzmann constant, and h is the Planck constant.

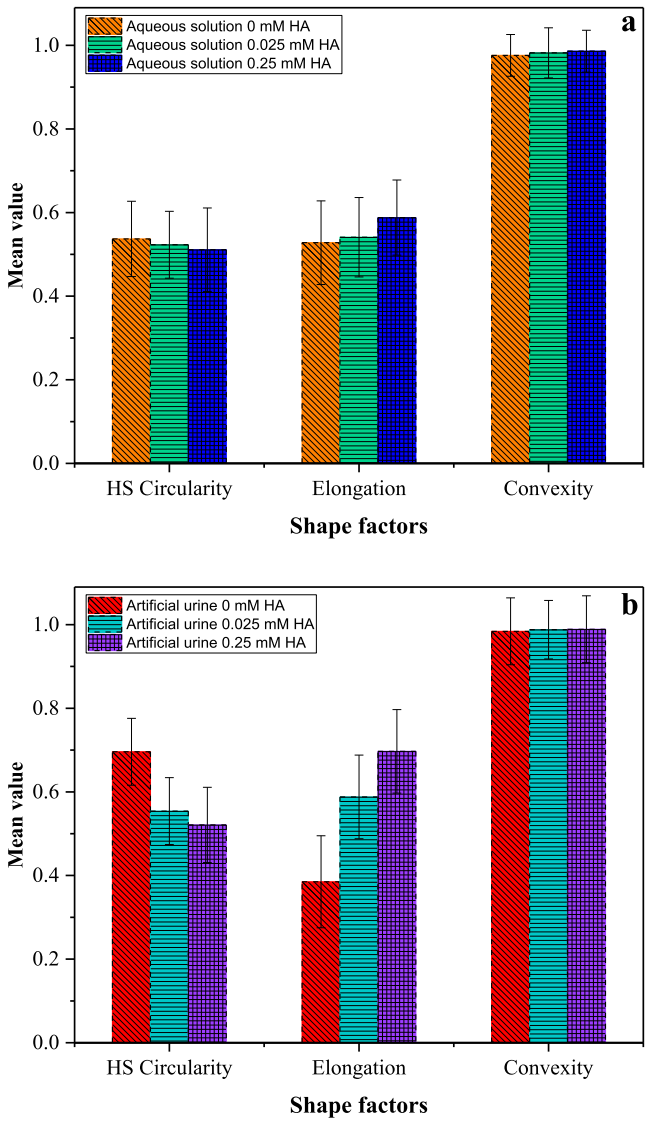

Fig. 4. Variation in shape factor values for the struvite crystals obtained in a) aqueous solution and b) artificial urine media.

3. Results and discussion

3.1. X-ray diffraction and Fourier transform infrared analyses

Fig. 1a shows the X-ray diffraction (XRD) patterns for the struvite crystals obtained in aqueous solution and the artificial urine media with and without hyaluronic acid. According to the XRD results, all diffraction peaks of the samples indicated that struvite was the only crystalline product without any traces of other impurities or any phases within the accuracy of XRD, which is consistent with the International Centre for Diffraction Data card no: 1–077-2303. Adding different concentrations of hyaluronic acid had no effect on crystal formation and no new crystallization products were observed. These results were also checked using Rietveld refinement analysis, which proved that all samples obtained were only the struvite form. The prominent diffraction peaks were detected at 2θ of 15.07, 15.89, 16.57, 20.86, 21.46, 27.16, 30.48, and 33.18° and corresponded to the (1 0 1), (0 0 2), (0 1 1), (1 1 1), (0 1 2), (1 0 3), (0 0 4), and (0 2 2) lattice planes of the struvite, respectively. The crystal system was an orthorhombic structure with space group $Pmn2_1$. Moreover, unit cell parameters of the struvite crystals were determined using materials analysis and diffraction (Table 2). These results were consistent with those reported from earlier studies [32–35].

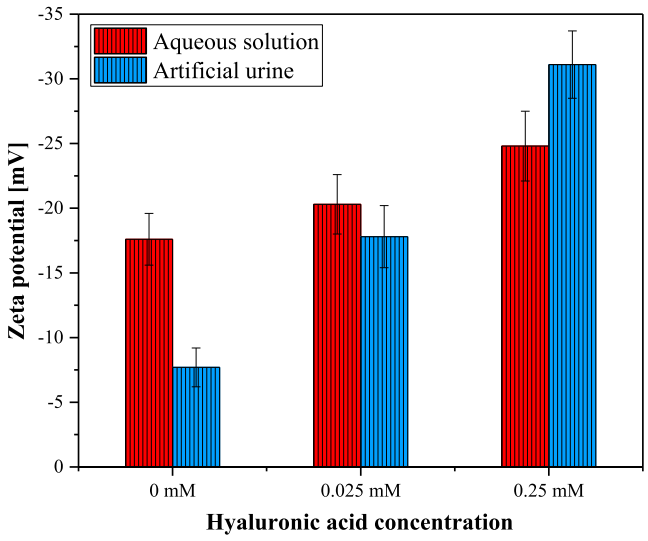

Fig. 5. The zeta (ζ) potentials of the struvite crystals as a function of hyaluronic acid concentration.

The XRD results obtained were confirmed by FTIR analysis (Fig. 1b). The FTIR spectra of the crystals obtained in aqueous solution and artificial urine using different concentrations of hyaluronic acid showed the main characteristic absorption peaks of struvite at 2890, 1430, 995, 875, and 750 cm^{-1}. The intensity and position of the major characteristic absorption peaks of the struvite crystals in the FTIR spectra were largely similar to those of struvite crystals reported in previous studies [2,36–39]. The characteristic peaks of other groups related to the hyaluronic acid were not observed within the working concentrations, which may have been a result of the small amounts of the adsorption of the modifier on the crystal surfaces that are beyond the detection ranges of the instrument used. In other words, this result demonstrated that struvite failed to form new chemical bonds with hyaluronic acid and therefore hyaluronic acid may function only on the surfaces of struvite crystals via physical adsorption. As shown in Fig. 1b, the broad peaks between ~ 3600 and ~ 2700 cm^{-1} were attributed to O–H stretching vibrations, indicating the presence of water, and symmetric and asymmetric stretching vibrations of N–H in NH_4^+ group. In addition, the peaks detected at ~2340 and ~1650 cm^{-1} were assigned to the H–O–H stretching vibrations of clusters of water molecules of crystallization and H–O–H bending molecules of vibrations, respectively. The peak at ~ 1430 cm^{-1} was associated with NH_4^+ asymmetric bending. In addition, the peak at 995 cm^{-1} was from the absorption of an asymmetrical stretching vibration of the phosphate (PO_4^{3-}). The ammonium–water H bonding and water–water H bonding were observed at 875 and 750 cm^{-1}, respectively. Overall, the FTIR spectra indicated that the struvite crystals obtained in aqueous solution and artificial urine using different concentrations of hyaluronic acid included the three basic characteristic peaks of crystalline water, NH_4^+ and phosphate.

3.2. Scanning electron microscopy analyses

The morphological properties of the struvite crystals were investigated using scanning electron microscopy (SEM). According to the theoretical fundamentals of crystal growth, the morphology depends on the relative growth rates of different crystal faces, which can change with variation in the solution environment and using a crystal modifier. Figs. 2 and 3 show the SEM images and particle-size distribution curves of the struvite crystals grown in aqueous solution and artificial urine media with and without hyaluronic acid, respectively.

The SEM image in Fig. 2a illustrates that the struvite grown in aqueous solution without hyaluronic acid consisted mainly of prismatic crystals with a rough surface. SEM images also reveal that the struvite

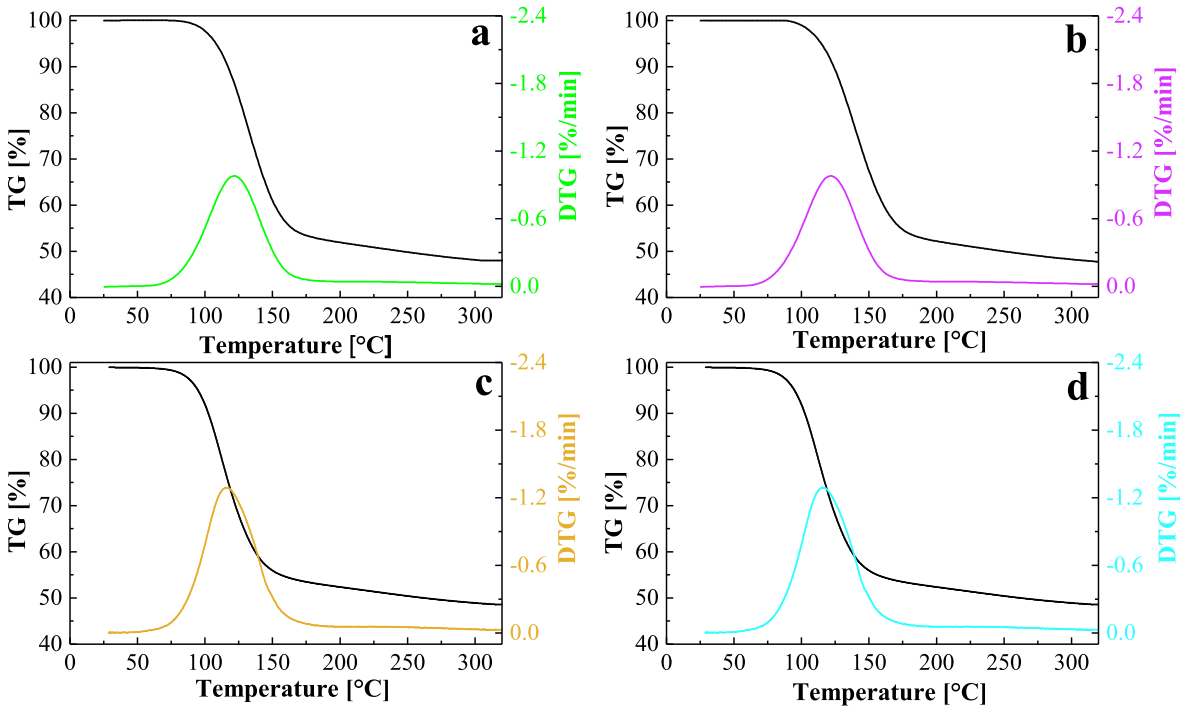

Fig. 6. Thermogravimetric analysis (TGA) and derivative thermogravimetry (DTG) curves for struvite crystals obtained in a) aqueous solution with 0 mM, and b) 0.25 mM hyaluronic acid; in c) artificial urine media with 0 mM, and d) 0.25 mM hyaluronic acid.

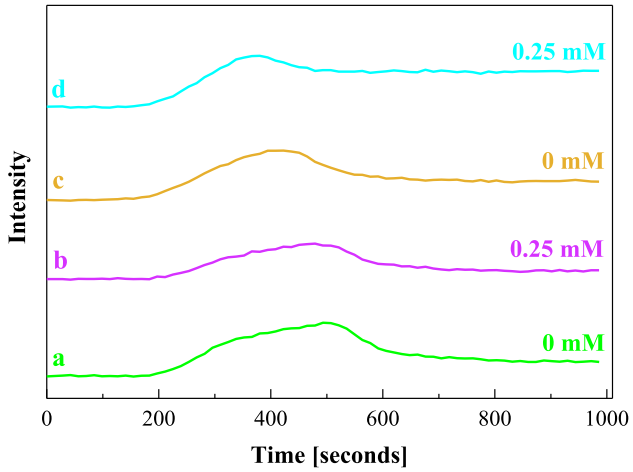

Fig. 7. Gram-Schmidt curves for struvite crystals obtained in a) aqueous solution with 0 mM, and b) 0.25 mM hyaluronic acid; in c) artificial urine media with 0 mM, and d) 0.25 mM hyaluronic acid.

crystals tend to grow on each other. Smaller crystals were formed on the surface of the larger crystals, which indicated that the crystals agglomerated in solution or during sample preparation step. Another possibility is secondary nucleation where secondary crystals nucleated on existing crystals due to impact with surrounding walls, other crystals or stirrer due to mixing. The SEM image in Fig. 2b shows that adding hyaluronic acid to the aqueous solution led to the variations in size of the struvite crystals. When the hyaluronic acid concentration was increased, the habit of the struvite remained in the prism form, just as those formed in the absence of hyaluronic acid, but the length and width of the crystals became smaller. In other words, resulting crystals became narrower and thinner in the presence of hyaluronic acid. Moreover, as seen in Fig. 2c, twinning formations that resulted in clustering were observed on the crystal surfaces and the crystals tended to grow on each other.

To date, struvite crystal growing in urine was investigated from different points of view. Although it takes a coffin-like habit, its morphology is affected by various physicochemical parameters, such as pH, supersaturation, and operation conditions such as stirring rate [3,40,41]. The struvite crystals grown in artificial urine without hyaluronic acid appeared in the form of large, rounded, compact agglomerates (Fig. 2d) and were deposited on the surface of the crystals. That is, the struvite crystals were different particle sizes were inlaid or adsorbed to form an agglomerated structure. Although the struvite crystals continued to grow on each other, their agglomeration tendencies were significantly reduced by 0.025 mM adding hyaluronic acid to the media; twinning was also observed (Fig. 2e). The SEM image in Fig. 2f shows that the surface of the struvite crystals grown in artificial urine with 0.25 mM hyaluronic acid was regular, homogenous, and smooth and were prismatic with a nearly uniform size. Moreover, the agglomeration tendency decreased significantly, and the twinning behavior was similar to that in aqueous solution media. Despite the fact that we performed the experiments with deionized water and artificial urine, the composition of the human urine also includes the presence of macromolecules such as proteins, glycosaminoglycans etc. which can have a significant impact on inhibition. In other words, solution chemistry is different due to combined effect of ionic strength, protonation reactions, and soluble complex formation and the environment of human urine [22] may alter the conformations of hyaluronic acid changing how hyaluronic acid interacts with struvite crystals. Yet without detailed solution chemistry modeling considering the role of hyaluronic acid in solution chemistry, which is beyond the scope of this study, underlying physical mechanism of struvite crystallization remains an open question. Yet we will propose and discuss potential mechanism how this this complex background may influence struvite crystallization. The possibility might be that the adsorption of hyaluronic acid on distinct facets resulting in altering growth rate. We can test this hypothesis by quantifying the change in surface charge of crystals in the presence of hyaluronic acid.

To accurately describe the quantitative change in crystal morphology exhibited in SEM imaging and to gain more insight into the effects of hyaluronic acid on struvite shape, the shapes were thoroughly analyzed using Malvern Morphologi G3 equipment. Fig. 4 shows the

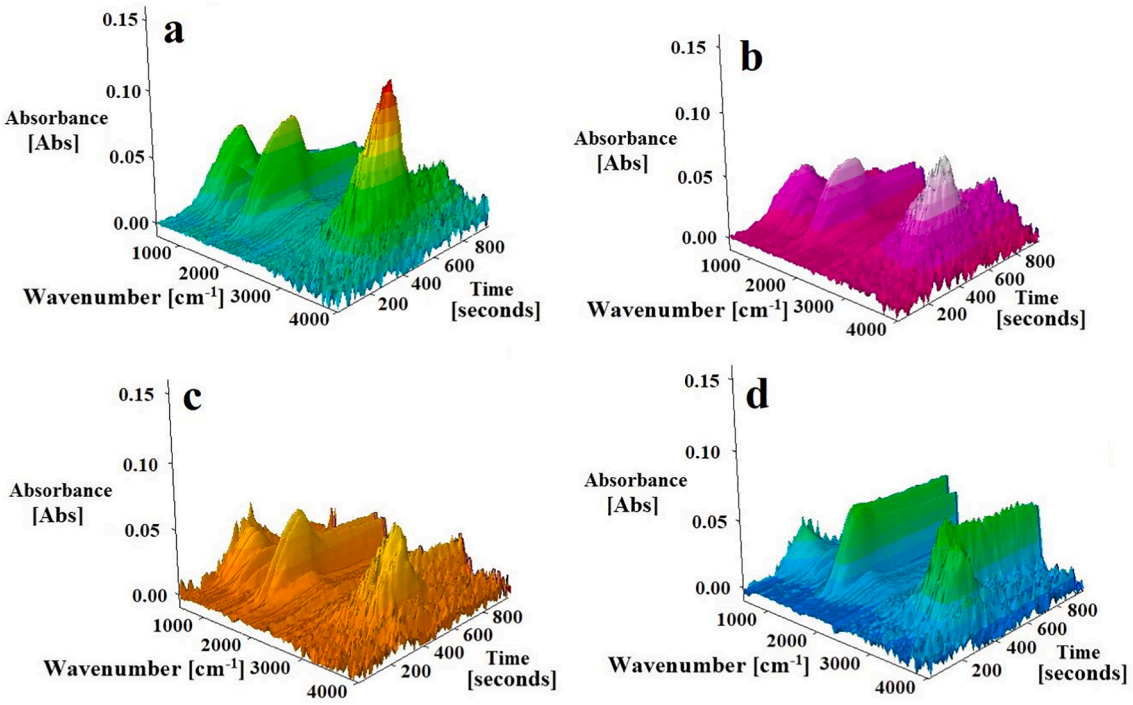

Fig. 8. Three-dimensional (3D) FTIR spectra for struvite crystals obtained in a) aqueous solution with 0 mM, and b) 0.25 mM hyaluronic acid; in c) artificial urine media with 0 mM, and d) 0.25 mM hyaluronic acid.

examination of widely used shape factors, such as circularity, elongation, and convexity value. "Circularity" refers to the ratio of the perimeter of a circle with the same area as the particle divided by the perimeter to the real particle image, or the "roundness" of a circle. The value of circularity ranges from 0 to 1. A perfect circle has a circularity of 1, but a "spiky" or irregular item has a circularity closer to 0. Circularity can be affected by both overall form and surface roughness. As a result, as the form grows rounder and smoother, the circularity approaches 1. The convexity of a particle describes its edge roughness, which is computed by dividing the convex hull perimeter by the actual particle perimeter. A smooth form has a convexity of 1, but a very spiky or irregular item has a convexity closer to 0. Elongation is calculated as 1-width/length; elongation ranges from 0 to 1. The elongation value of a symmetrical form (e.g., circle or square) in all directions is 0 and shapes with high aspect ratios have elongation values that are closer to 1. As the hyaluronic acid concentration increased from 0 to 0.25 mM, the elongation value increased from 0.528 ± 0.10 to 0.588 ± 0.09, and 0.385 ± 0.11 to 0.697 ± 0.10 in aqueous solution and artificial urine media, respectively. The elongation value for artificial urine media was higher than that of the struvite grown in the aqueous solution. In artificial urine media, the high sensitivity circularity value of the struvite obtained without hyaluronic acid was 0.696 ± 0.08; however, this value decreased to 0.521 ± 0.09 in 0.25 mM hyaluronic acid. The circularity value was expected to be low because the crystals formed in hyaluronic acid had a rod-like structure. On the other hand, the convexity value was observed to be between 0.976 ± 0.05 and 0.985 ± 0.05 and 0.984 ± 0.08 and 0.989 ± 0.08 in aqueous solution and artificial urine media, respectively, and was unaffected by hyaluronic acid concentration in either media. The agglomeration tendency under the working conditions was determined using aspect ratios obtained by dividing the crystal's width by its length. The aspect ratio value for artificial urine was 0.615 ± 0.11 in the absence of hyaluronic acid and decreased to 0.303 ± 0.10 after adding 0.25 mM hyaluronic acid. This indicated that the agglomeration behavior of the struvite decreased with increasing hyaluronic acid concentration, a result that is consistent with the images acquired from SEM analyses. These results indicated that crystal agglomeration decreased in terms of shape analyses.

Solidity, another morphological parameter, is found by dividing an object's area into areas enclosed by a convex hull area. The solidity values are 1 for morphologically very smooth, rounded shapes. The average solidity value calculated for struvite crystals obtained without hyaluronic acid in artificial urine was 0.983, while this value decreased to 0.919 with the increased concentration of the modifier.

To summarize, hyaluronic acid had a significant impact on the shape and size of the struvite crystals. Based on the results of SEM images and shape analyses, hyaluronic acid had a favorable effect on the struvite crystals by modifying their shape and reducing their size and agglomeration tendency. Several hypotheses have been put forward to explain the mechanism through which modifiers affect struvite crystallization. The modifiers are capable of changing significantly the surface of crystals through chemical bonding or physical attachment onto the surfaces [42–44]. Hyaluronic acid, used as a crystal modifier in this study, is a high-molecular-mass polysaccharide and the size, negative ionic charge, and ability to form hydrated gel-like matrices make hyaluronic acid a significant crystal-binding molecule. In addition, the anionic nature of hyaluronic acid allows for complex interaction with cations [45,46]. On the basis of the experimental data, we can suggest that hyaluronic acid interacts with struvite crystals by physical adsorption rather than through chemical bonding and affect the growth rate of crystals by occupying the active growth sites on the surfaces of struvite. The physical adsorption mainly includes electrostatic interaction, dispersion force, and hydrogen bonding formation. Among these, the electrostatic interaction has an important influence on the struvite adsorption process. Due to the anionic nature [46,47], hyaluronic acid has abundant negatively charged carboxyl groups and they can bind the positively charged groups at the struvite surface and thus reducing struvite deposits or selectively hindering the growth of particular crystal faces.

3.3. Zeta potential analysis

The zeta (ζ) potential was a useful tool for determining the surface charge and stability of the samples and helps to explain their

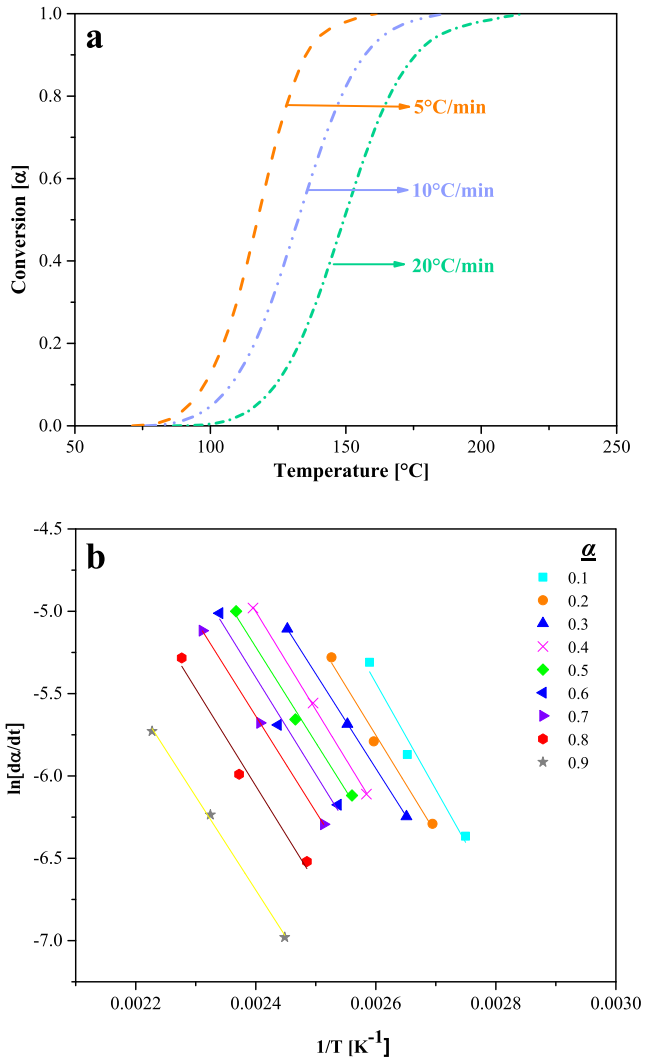

Fig. 9. a) Conversion vs. temperature at different heating rates, and b) plot of Friedman method for struvite crystals.

Table 3
The kinetic and thermodynamic parameters for thermal decomposition of struvite crystals.

Conversion α	E (kJ/mol)	R^2	A (min^{-1})	ΔH (kJ/mol)	ΔG (kJ/mol)	ΔS (J/mol.K)
0.1	53.8	0.9756	1.14×10^7	50.6	97.1	−118.0
0.2	49.5	0.9903	2.76×10^6	46.2	98.5	−132.8
0.3	47.7	0.9999	1.56×10^6	44.3	100.2	−141.7
0.4	49.7	0.9995	2.95×10^6	46.2	101.2	−139.5
0.5	48.2	0.9924	1.85×10^6	44.7	102.0	−145.3
0.6	49.0	0.9893	2.38×10^6	45.5	102.5	−144.7
0.7	48.3	0.9990	1.91×10^6	44.7	103.3	−148.5
0.8	49.0	0.9830	2.38×10^6	45.4	104.0	−148.7
0.9	47.2	0.9985	1.32×10^6	43.5	105.6	−157.6
Average	49.2 ± 5.1		3.17×10^6	45.7	101.6	−141.9

agglomeration tendency [48]. Fig. 5 shows the ζ potential of the struvite crystals grown in aqueous solution and artificial urine as a function of hyaluronic acid concentration.

The struvite crystals grown in aqueous solution had a ζ potential of −17.6 ± 2.0 mV. As shown in Fig. 5, the ζ potential of the struvite crystals was highly affected by the hyaluronic acid and increased with an increase in its concentration. When the hyaluronic acid concentration was 0.25 mM, the crystals were negatively charged, with a ζ potential of −24.8 ± 2.7 mV. A similar outcome was observed for the struvite crystals grown in artificial urine. The ζ potential of the crystals without hyaluronic acid had a negative value of −7.7 ± 1.5 mV. After adding 0.25 mM hyaluronic acid to the media, the surface charge significantly decreased to −31.1 ± 2.6 mV. The ζ potential is a key indicator of the stability of a suspension of particles. As a general rule, particles in suspension at + 30 mV > ζ > − 30 mV are considered to be stable [37], which indicates that particles with a ζ potential>+30 mV or < -30 mV are normally considered stable while those with a ζ potential from − 30 to + 30 mV tend to aggregate; therefore, we suggest that the struvite crystals obtained in hyaluronic acid were highly stable, and that the changes in ζ potential may suggest van der Waals interaction induced adsorption of the hyaluronic acid on the surface of the struvite crystals.

3.4. TGA–FTIR analyses

Thermogravimetric analysis produces fast and quantitative results and thus has been used extensively to analyze kidney stones. The TGA and derivative thermogravimetry (DTG) curves for the struvite crystals grown in aqueous solution and artificial urine media with and without hyaluronic acid at a heating rate of 20 °C/min are shown in Fig. 6.

As shown in Fig. 6, the decreased weight of the struvite crystals grown in aqueous solution was 51.5% at 325 °C, which was close to the theoretical value (51.4%). As stated in the literature [49–51], thermal decomposition of the struvite crystals included one main stage that was simultaneous with a decrease of 44.08% H_2O (dehydration) and the liberation of 7.34% NH_3. A similar trend was observed for the struvite crystals grown in artificial urine. The residue amount at 325 °C was 48.5 wt%, which agreed with the theoretical value. As shown in the TG/DTG curves for the struvite crystals, the hyaluronic acid had no significant effect on the thermal decomposition mechanism.

A logical interpretation for the thermal mechanism by which struvite crystals decompose, which involves the formation of gaseous species, depends greatly on the molecular characterization of the evolved products [52]; therefore, using TGA/FTIR is helpful for determining the thermal properties and identifying a simultaneous release of volatile components. Using this combination, a thorough understanding of the nature of the thermal decomposition processes is feasible. Fig. 7 shows the Gram–Schmidt curves of the overall FTIR absorbance values of the gases generated during the thermal decomposition process at a heating rate of 20 °C/min, and quantitatively displays the total infrared absorption depending on vector analysis of the obtained interferograms (i.e., they demonstrate how the concentrations of the evolved gases change throughout the thermal decomposition process). Although there were instances of small-time delays because of the volatile transportation from TG to FTIR, the Gram–Schmidt curves resembled the DTG curves and correlated directly with the stage in the TGA curves. In addition, the three-dimensional (3D) FTIR spectra for the struvite crystals obtained in aqueous solution and artificial urine with and without hyaluronic acid are shown in Fig. 8 to demonstrate the variance in spectral intensity across time and wavelength. As can be seen from the 3D spectra, the main and most intensive absorbance peak between 58 and 195 °C corresponded to O–H stretching vibrations was within the region of 3500–2700 cm^{-1} was attributed to the removal of H_2O from the struvite crystals. In addition, another peak detected about 1000 cm^{-1} indicated the removal of NH_3 from the struvite crystals. Although the peak intensities changed slightly, this result was similar to that of the struvite crystals grown in artificial urine media with and without hyaluronic

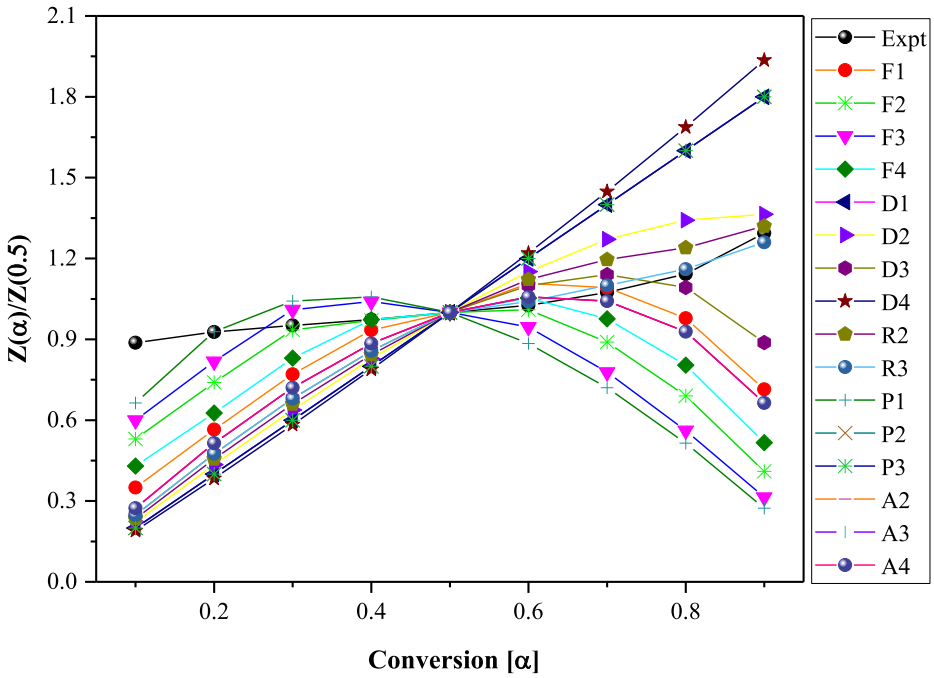

Fig. 10. Theoretical and experimental master plots for thermal decomposition of struvite crystals.

acid. Based on TGA/FTIR results, water and ammonia were main volatile products that evolved.

3.5. Kinetic and thermodynamic analyses

In this study, we used the Friedman method to determine the activation energy of the struvite crystals obtained in aqueous solution using three different heating rates. As shown in Fig. 9, the straight lines were obtained first and then the values of the activation energy as a function of the conversion range from 0.1 to 0.9 were computed from the slopes using the linear model equation. The high correlation coefficient (>0.95) values for straight lines in the Friedman plots indicated the success of this method in explaining the kinetics of struvite thermal decomposition. The calculated activation energies and frequency factors were tabulated (Table 3); the activation energy denoted the minimum amount of energy required to initiate the process. As a result, the larger the activation energy, the more difficult the reaction and the lower the activation energy, the less energy it takes to breakdown the chemical bonds, and thus the more easily the associated reaction can be conducted. A comparatively large activation energy, on the other hand, suggests a greater temperature necessary to breakdown the structure. At varying conversion degrees, approximately the same activation energy values are assigned to identical kinetic behavior, most likely the same chemical process; however, higher discrepancies and variations in activation energy levels at various conversion degrees imply that the entire conversion process is governed by separate mechanisms. Moreover, the parallelism behavior of the straight lines is associated with the similar kinetic behavior and probably the same reaction mechanisms. The average activation energy of the struvite crystals using the Friedman method was 49.2 ± 5.1 kJ/mol. The estimated value of the activation energy was similar to that found in previous work [53]. Also similar to that found in the literature [8] were the calculated frequency factors that were within the range of 1.32×10^6–1.14×10^7 min^{-1}, with an average of 3.17×10^6 for conversions of 0.1 to 0.9 at a heating rate of 20 °C/min. As shown in Table 3, the activation energy slightly changed as a function of conversion degree, which was attributed to a multiple stage reaction mechanism during the decomposition process owing to the dehydration of the crystal water and releasing of ammonia occurring simultaneously [54].

To determine the predominant reaction mechanism involved in the thermal decomposition of struvite crystals at different levels of conversion at a heating rate of 20 °C/min, we used Z(α)/Z(0.5) curves generated using different reaction mechanisms (Table 1). Fig. 10 shows the experimental and theoretical master plots used. We specified the theoretical curve closest to the experimental curve as the dominant mechanism. The thermal kinetics that we calculated using the second order reaction mechanism (the F_2 type model) agreed with the experimental data at lower conversion degree. At α = 0.6, the experimental curve showed a variation in its shape. For the interval of α = 0.6–0.9, the mechanism closely followed the contracting sphere mechanism (the R_3 type model).

In addition to the analysis of thermal kinetics, a proper assessment of the thermodynamic parameters, such as the Gibbs free-energy change (ΔG), enthalpy change (ΔH), and entropy change (ΔS), could provide in-depth information about the nature of the thermal decomposition of struvite crystals; therefore, these parameters were calculated, and the results as a function of conversion are provided in Table 3. ΔH is a vital factor for assessing whether the adsorption process is endothermic or exothermic based on a positive or negative value. The ΔH for the thermal decomposition of struvite crystals varied from 43.5 to 50.6 kJ/mol. The average enthalpy value was 45.7 kJ/mol, which indicated that the decomposition process was endothermic and was similar to the those calculated in the previous study [55]. The entropy changes for the crystals were within the range of − 118.0 to − 157.6 J/mol K. Theoretically, ΔS can provide information on system disorders during the thermal decomposition process and a negative value indicates that the degree of disorder of the system is reduced, and that the system is moving toward the equilibrium state. Low or negative entropy values indicate thermal equilibrium for the reaction after various physicochemical changes. The lowest negative value of ΔS was − 118.0 J/mol K at a conversion degree of 0.1. ΔG is a critical factor in determining the degree of spontaneity in thermodynamic reactions. These values were within the range of 97.1 and 105.6 kJ/mol. For all conversion degrees, ΔG was positive, which indicated that the process was neither feasible nor spontaneous.

4. Conclusion

In the present study, the effect of hyaluronic acid on struvite crystallization was examined in aqueous solution and artificial urine media. The results of XRD and FTIR showed that the products obtained with and without hyaluronic acid were struvite crystals, and SEM analysis showed that hyaluronic acid had significant effects on the size and morphology of the crystals. The struvite crystals revealed a homogenous surface of larger agglomerated crystals in artificial urine media, while the hyaluronic acid created smaller, regular, prismatic struvite crystals. These observations revealed the variation of the shape parameters, confirmed by particle shape analysis. The elongation value increased from 0.385 ± 0.11 to 0.697 ± 0.10 in artificial urine media after adding hyaluronic acid. The results of the ζ potential measurements illustrated that the struvite crystals were negatively charged, and that hyaluronic acid could be adsorbed on their surfaces, thus the negativity of the surface charge increased in both aqueous solution and artificial urine media. The Friedman method was used to investigate the kinetic parameters, and thermal decomposition mechanism of the struvite was assessed at different conversion levels. The activation energy for decomposition was within the range of 47.2–53.8 kJ/mol, with an average value of 49.2 ± 5.1 kJ/mol. The results revealed that the combination of the second order reaction mechanism (F_2) and the contracting sphere mechanism (R_3) are more suitable mechanisms by which to describe the thermal characteristics of the struvite. Furthermore, we calculated the thermodynamic parameters resulting in ΔH and ΔG of 45.7 and 101.6 kJ/mol, respectively, which indicated an endothermic and nonspontaneous thermal decomposition process. Finally, the present study provides a general impression of the modified crystal morphology, and a reduction in the struvite crystals that resulted from using hyaluronic acid. We believe that these results will improve the understanding of how hyaluronic acid alters struvite crystallization. This information could be significant for developing effective and non-invasive treatment for infection stones.

CRediT authorship contribution statement

Sevgi Polat: Conceptualization, Methodology, Investigation, Validation, Visualization, Writing – original draft, Writing – review & editing. **Huseyin Burak Eral:** Conceptualization, Visualization, Writing – original draft, Writing – review & editing, Supervision.

Declaration of Competing Interest

The authors declare that they have no known competing financial interests or personal relationships that could have appeared to influence the work reported in this paper.

References

[1] L. Estepa, M. Daudon, Contribution of Fourier Transform Infrared Spectroscopy (1997) 347–369.

[2] D. Bazin, G. André, R. Weil, G. Matzen, V. Emmanuel, X. Carpentier, M. Daudon, Absence of bacterial imprints on struvite-containing kidney stones: A structural investigation at the mesoscopic and atomic scale, Urology. 79 (4) (2012) 786–790, https://doi.org/10.1016/j.urology.2011.08.054.

[3] J. Prywer, A. Torzewska, Bacterially induced struvite growth from synthetic urine: Experimental and theoretical characterization of crystal morphology, Cryst. Growth Des. 9 (8) (2009) 3538–3543, https://doi.org/10.1021/cg900281g.

[4] J. Prywer, R.R. Sadowski, A. Torzewska, Aggregation of struvite, carbonate apatite, and Proteus mirabilis as a key factor of infectious urinary stone formation, Cryst. Growth Des. 15 (3) (2015) 1446–1451, https://doi.org/10.1021/cg5018032.

[5] P. Das, G. Gupta, V. Velu, R. Awasthi, K. Dua, H. Malipeddi, Formation of struvite urinary stones and approaches towards the inhibition—A review, Biomed. Pharmacother. 96 (2017) 361–370, https://doi.org/10.1016/j.biopha.2017.10.015.

[6] L. Chen, Y. Shen, A. Xie, F. Huang, W. Zhang, S. Liu, Seed-mediated synthesis of unusual struvite hierarchical superstructures using bacterium, Cryst. Growth Des. 10 (5) (2010) 2073–2082, https://doi.org/10.1021/cg900974n.

[7] J. Prywer, L. Sieroń, A. Czylkowska, Struvite grown in gel, its crystal structure at 90 k and thermoanalytical study, Crystals. 9 (2) (2019) 89, https://doi.org/10.3390/cryst9020089.

[8] C.K. Chauhan, M.J. Joshi, In vitro crystallization, characterization and growth-inhibition study of urinary type struvite crystals, J. Cryst. Growth. 362 (2013) 330–337, https://doi.org/10.1016/j.jcrysgro.2011.11.008.

[9] P.D. Rekha, A. Hameed, M.A.P. Manzoor, M.V. Suryavanshi, S.D. Ghate, A.B. Arun, S.S. Rao, Athmika, S.K. Bajire, M. Mujeeburahiman, C.-C. Young, First report of pathogenic bacterium kalamiella piersonii isolated from urine of a kidney stone patient: Draft genome and evidence for role in struvite crystallization, Pathogens. 9 (9) (2020) 711, https://doi.org/10.3390/pathogens9090711.

[10] R. Flannigan, W.H. Choy, B. Chew, D. Lange, Renal struvite stones - Pathogenesis, microbiology, and management strategies, Nat. Rev. Urol. 11 (6) (2014) 333–341, https://doi.org/10.1038/nrurol.2014.99.

[11] M. Olszynski, J. Prywer, E. Mielniczek- Brzóska, Inhibition of Struvite Crystallization by Tetrasodium Pyrophosphate in Artificial Urine: Chemical and Physical Aspects of Nucleation and Growth, Cryst. Growth Des. 16 (6) (2016) 3519–3529, https://doi.org/10.1021/acs.cgd.6b0048710.1021/acs.cgd.6b00487.s001.

[12] J. Prywer, M. Olszynski, E. Mielniczek Brzóska, Green Tea and Struvite Crystals in Relation to Infectious Urinary Stones: The Role of (-)-Epicatechin, Cryst. Growth Des. 17 (11) (2017) 5953–5964, https://doi.org/10.1021/acs.cgd.7b01043.

[13] M.A.P. Manzoor, M. Mujeeburahiman, S.R. Duwal, P.D. Rekha, Investigation on growth and morphology of in vitro generated struvite crystals, Biocatal. Agric, Biotechnol. 17 (2019) 566–570, https://doi.org/10.1016/j.bcab.2019.01.023.

[14] J. Prywer, E. Mielniczek-Brzóska, Effect of (-)-Epicatechin on Poorly Crystalline and Amorphous Precipitate. The Role of Green Tea Compound in the Formation of Infectious Urinary Stones, Cryst. Growth Des. 20 (1) (2020) 148–156, https://doi.org/10.1021/acs.cgd.9b00936.

[15] D. Kim, C. Olympiou, C.P. McCoy, N.J. Irwin, J.D. Rimer, Time-Resolved Dynamics of Struvite Crystallization: Insights from the Macroscopic to Molecular Scale, Chem. - A Eur. J. 26 (16) (2020) 3555–3563, https://doi.org/10.1002/chem.201904347.

[16] J. Prywer, A. Torzewska, Effect of curcumin against proteus mirabilis during crystallization of struvite from artificial urine, Evidence-Based Complement. Altern. Med. 2012 (2012) 1–7, https://doi.org/10.1155/2012/862794.

[17] B. Kaleeswaran, S. Ramadevi, R. Murugesan, S. Srigopalram, T. Suman, T. Balasubramanian, Evaluation of anti-urolithiatic potential of ethyl acetate extract of Pedalium murex L. on struvite crystal (kidney stone), J. Tradit. Complement. Med. 9 (1) (2019) 24–37, https://doi.org/10.1016/j.jtcme.2017.08.003.

[18] P. Das, K. Kumar, A. Nambiraj, R. Awasthi, K. Dua, H. Malipeddi, Antibacterial and In Vitro Growth Inhibition Study of Struvite Urinary Stones Using Oxalis corniculata Linn. Leaf Extract and its Biofabricated Silver Nanoparticles, Recent Pat, Drug Deliv. Formul. 12 (3) (2019) 170–178, https://doi.org/10.2174/1872211312666180723160624.

[19] O. Masala, P. O'Brien, G. Rafeletos, Formation of Spherical Granules of Calcium Pyrophosphate, Cryst. Growth Des. 3 (3) (2003) 431–434, https://doi.org/10.1021/cg020064g.

[20] F. Martinon, V. Pétrilli, A. Mayor, A. Tardivel, J. Tschopp, Gout-associated uric acid crystals activate the NALP3 inflammasome, Nature. 440 (7081) (2006) 237–241, https://doi.org/10.1038/nature04516.

[21] M. Asselman, A. Verhulst, E.S. Van Ballegooijen, C.H. Bangma, C.F. Verkoelen, M. E. De Broe, Hyaluronan is apically secreted and expressed by proliferating or regenerating renal tubular cells, Kidney Int. 68 (1) (2005) 71–83, https://doi.org/10.1111/j.1523-1755.2005.00382.x.

[22] S. Polat, H. Burak Eral, Elucidating the role of hyaluronic acid in the structure and morphology of calcium oxalate crystals, Adv. Powder Technol. 32 (10) (2021) 3650–3659, https://doi.org/10.1016/j.apt.2021.08.021.

[23] N.W. Poon, M.D.I. Gohel, Urinary glycosaminoglycans and glycoproteins in a calcium oxalate crystallization system, Carbohydr. Res. 347 (1) (2012) 64–68, https://doi.org/10.1016/j.carres.2011.09.022.

[24] C.-A. Lamontagne, G.E. Plante, M. Grandbois, Characterization of hyaluronic acid interaction with calcium oxalate crystals: implication of crystals faces, pH and citrate, J. Mol. Recognit. 24 (4) (2011) 733–740, https://doi.org/10.1002/jmr.1110.

[25] W. Dong, Q. Wu, Dual Roles of Melamine in the Formation of Calcium Oxalate Stones, Cryst. Growth Des. 19 (7) (2019) 3998–4007, https://doi.org/10.1021/acs.cgd.9b0038910.1021/acs.cgd.9b00389.s001.

[26] O. Miyake, K. Yoshimura, T. Yoshioka, T. Koide, A. Okuyama, High urinary excretion level of citrate and magnesium in children: Potential etiology for the reduced incidence of pediatric urolithiasis, Urol. Res. 26 (3) (1998) 209–213, https://doi.org/10.1007/s002400050048.

[27] H.L. Friedman, Kinetics of thermal degradation of char-forming plastics from thermogravimetry. Application to a phenolic plastic, J. Polym. Sci. Part C. 6 (1) (1964) 183–195, https://doi.org/10.1002/polc.5070060121.

[28] H. Kissinger, Variation of peak temperature with heating rate in differential thermal analysis, J. Res. Natl. Bur. Stand. 57 (1956) (1934) 217–221, https://doi.org/10.1002/9781119959809.ch9.

[29] J.M. Criado, Kinetic analysis of DTG data from master curves, Thermochim. Acta. 24 (1) (1978) 186–189.

[30] H. Eyring, The activated complex in chemical reactions, J. Chem. Phys. 3 (2) (1935) 107–115, https://doi.org/10.1063/1.1749604.

[31] M.G. Evans, M. Polanyi, Some applications of the transition state method to the calculation of reaction velocities, especially in solution, Trans. Faraday Soc. 31 (1935) 875–894, https://doi.org/10.1039/tf9353100875.

[32] B. Gu, J. Schmitt, Z. Chen, L. Liang, J.F. McCarthy, Adsorption and Desorption of Natural Organic Matter on Iron Oxide, Mechanisms and Models 28 (1) (1994) 38–46.
[33] J. Prywer, A. Torzewska, Biomineralization of struvite crystals by Proteus mirabilis from artificial urine and their mesoscopic structure, Cryst. Res. Technol. 45 (2010) 1283–1289, https://doi.org/10.1002/crat.201000344.
[34] L. Qin, C.V. Putnis, L. Wang, Facet-Specific Dissolution-Precipitation at Struvite-Water Interfaces, Cryst. Growth Des. 21 (7) (2021) 4111–4120, https://doi.org/10.1021/acs.cgd.1c0040010.1021/acs.cgd.1c00400.s001.
[35] T. Hong, L. Wei, K. Cui, T. Chen, L. Luo, M. Fu, Q. Zhang, A constant composition technique for quantifying the effect of As(V) on struvite crystallization under various operational conditions, J. Cryst. Growth. 552 (2020) 125925, https://doi.org/10.1016/j.jcrysgro.2020.125925.
[36] B. Tansel, G. Lunn, O. Monje, Struvite formation and decomposition characteristics for ammonia and phosphorus recovery: A review of magnesium-ammonia-phosphate interactions, Chemosphere. 194 (2018) 504–514, https://doi.org/10.1016/j.chemosphere.2017.12.004.
[37] V. Uskoković, Dynamic Light Scattering Based Microelectrophoresis: Main Prospects and Limitations, J. Dispers. Sci. Technol. 33 (12) (2012) 1762–1786, https://doi.org/10.1080/01932691.2011.625523.
[38] R. Rajan, N.A.N. Raj, S. Madeswaran, D.R. Babu, Dielectric studies on struvite urinary crystals, a gateway to the new treatment modality for urolithiasis, Spectrochim. Acta - Part A Mol. Biomol. Spectrosc. 148 (2015) 266–270, https://doi.org/10.1016/j.saa.2015.03.136.
[39] Y. Luo, H. Li, Y.R. Huang, T.L. Zhao, Q.Z. Yao, S.Q. Fu, G.T. Zhou, Bacterial mineralization of struvite using MgO as magnesium source and its potential for nutrient recovery, Chem. Eng. J. 351 (2018) 195–202, https://doi.org/10.1016/j.cej.2018.06.106.
[40] A. Wierzbicki, J.D. Sallis, E.D. Stevens, M. Smith, C.S. Sikes, Crystal growth and molecular modeling studies of inhibition of struvite by phosphocitrate, Calcif. Tissue Int. 61 (3) (1997) 216–222, https://doi.org/10.1007/s002239900326.
[41] R.R. Sadowski, J. Prywer, A. Torzewska, Morphology of struvite crystals as an evidence of bacteria mediated growth, Cryst. Res. Technol. 49 (7) (2014) 478–489, https://doi.org/10.1002/crat.201400080.
[42] N.P. Rao, G.M. Preminger, J.P. Kavanagh (Eds.), Urinary Tract Stone Disease, Springer London, London, 2011.
[43] A. Lewis, M. Seckler, H. Kramer, G. Van Rosmalen, Industrial Crystallization Fundementals and Applications, Cambridge University Press, 2015.
[44] K. Suguna, M. Thenmozhi, C. Sekar, Growth, spectral, structural and mechanical properties of struvite crystal grown in presence of sodium fluoride, Bull. Mater. Sci. 35 (4) (2012) 701–706.
[45] A. Verhulst, M. Asselman, V.P. Persy, M.S.J. Schepers, M.F. Helbert, C. F. Verkoelen, M.E.D.E. Broe, Crystal Retention Capacity of Cells in the Human Nephron : Involvement of CD44 and Its Ligands Hyaluronic Acid and Osteopontin in the Transition of a Crystal Binding- into a Nonadherent Epithelium, J. Am. Soc. Nephrol. 13 (2003) 107–115, https://doi.org/10.1097/01.ASN.0000038686.17715.42.
[46] K.P. Aggarwal, S. Narula, M. Kakkar, C. Tandon, Nephrolithiasis : Molecular Mechanism of Renal Stone Formation and the Critical Role Played by Modulators, Biomed Res. Int. 2013 (2013) 1–21. https://doi.org/https://doi.org/10.1155/2013/292953.
[47] Z.-H. Chen, X.-L. Ren, H.-H. Zhou, X.-D. Li, The role of hyaluronic acid in biomineralization, Front, Mater. Sci. 6 (4) (2012) 283–296, https://doi.org/10.1007/s11706-012-0182-4.
[48] M. Fromberg, M. Pawlik, D.S. Mavinic, Induction time and zeta potential study of nucleating and growing struvite crystals for phosphorus recovery improvements within fluidized bed reactors, Powder Technol. 360 (2020) 715–730, https://doi.org/10.1016/j.powtec.2019.09.067.
[49] M.I.H. Bhuiyan, D.S. Mavinic, F.A. Koch, Thermal decomposition of struvite and its phase transition, Chemosphere. 70 (8) (2008) 1347–1356, https://doi.org/10.1016/j.chemosphere.2007.09.056.
[50] R.L. Frost, M.L. Weier, K.L. Erickson, Thermal decomposition of struvite: Implications for the decomposition of kidney stones, J. Therm. Anal. Calorim. 76 (3) (2004) 1025–1033, https://doi.org/10.1023/B:JTAN.0000032287.08535.b3.
[51] J. Hövelmann, T.M. Stawski, R. Besselink, H.M. Freeman, K.M. Dietmann, S. Mayanna, B.R. Pauw, L.G. Benning, A template-free and low temperature method for the synthesis of mesoporous magnesium phosphate with uniform pore structure and high surface area, Nanoscale. 11 (14) (2019) 6939–6951.
[52] S. Materazzi, S. Vecchio, Recent applications of evolved gas analysis by infrared spectroscopy (IR-EGA), Appl. Spectrosc. Rev. 48 (8) (2013) 654–689, https://doi.org/10.1080/05704928.2013.786722.
[53] E. Ariyanto, T.K. Sen, H.M. Ang, The influence of various physico-chemical process parameters on kinetics and growth mechanism of struvite crystallisation, Adv. Powder Technol. 25 (2) (2014) 682–694, https://doi.org/10.1016/j.apt.2013.10.014.
[54] A.A. Rouff, The use of TG/DSC-FT-IR to assess the effect of Cr sorption on struvite stability and composition, J. Therm. Anal. Calorim. 110 (3) (2012) 1217–1223, https://doi.org/10.1007/s10973-011-2101-9.
[55] C.K. Chauhan, K.C. Joseph, B.B. Parekh, M.J. Joshi, Growth and characterization of struvite crystals, Indian J. Pure Appl. Phys. 46 (2008) 507–512, https://doi.org/10.1002/crat.201000587.